Double-leaf masonry walls under in-plane loading strengthened with GFRP/SRG strips

Double-leaf masonry walls under in-plane loading strengthened with GFRP/SRG strips

by

R. Capozucca[1]

ABSTRACT

Multiple-leaf masonry walls are usually adopted in historic buildings in seismic areas. An investigation on this type of masonry wall, characterized by two leaves of brickwork masonry and intermediate grout, has been carried out on models in laboratory. Knowing how historic masonry behaves under seismic action is fundamental for preserving architectural heritage. During earthquakes, masonry walls are subjected to shear loads that often lead to the ruin of an entire building. In recent years, the strengthening of masonry walls often foresees external bonded fiber reinforced polymers (FRPs) even if many aspects of this technique are not thoroughly known. In particular, the debonding mechanisms of FRP strips needs to be analyzed using more experimental data.

This paper presents the results of an investigation on historic unreinforced double-leaf masonry wall models built with historic solid clay bricks in scale 1/3rd. The unreinforced models were tested under combined compression and shear loading; after damage they were strengthened with two types of external bonded composite materials – diagonal Glass-FRP strips and steel fiber reinforced cement grout (SRG) – and then once again subjected to the same loading until failure. A comparison between the response of the unreinforced and reinforced model is presented, and the failure debonding mechanisms of strengthened shear wall models with GFRP/SRG strips are discussed.

Keywords: Double-leaf masonry wall; strengthening; GFRP; SRG; shear test; debonding.

[1] Confirmed Assoc. Prof. of Struct.l Engineering, Struct.Section DICEA, Università Politecnica delle Marche, Ancona, ITALY, phone +39.071.2204570 fax +39.071.2204576 r.capozucca@univpm.it

1. INTRODUCTION

Historical masonry walls have often demonstrated weaknesses under earthquake motion, in particular, in the case of multiple-leaf masonry walls, as documented in various reports concerning damage due to the earthquakes which hit a number of Italian regions in the last few decades Umbria-Marche, 1997-98 [1]; L'Aquila, 2009; Emilia, 2012.

Knowledge regarding the behaviour of masonry walls under seismic action [2-5] is, without doubt, the basis for preserving architectural heritage as both monumental historic masonry buildings and/or minor masonry buildings. The preservation of architectural heritage presents a complexity driving from the geometry of the structures in question, the variability of the materials used, and the loading history of such buildings [6,7].

Because of their nature and history, structures of historic buildings present a number of typical, practical aspects that limit the application of modern codes and building standards [8]. Firstly, the shear strength of unreinforced masonry still requires investigation, although it has been analysed by many experimental works over the last decades [3-5, 9,10], even adopting different scale models [9,11], and theoretical modelling analysis [12]. Furthermore, for multiple-leaf masonry walls - usually adopted in historic buildings - behaviour under shear force is not commonly investigated [13,14,7] even if the common cause for damages during an earthquake is still attributable to this type of masonry; where the lack of ties between leaves and/or the deterioration of the materials lead to ruin.

In recent years, the rehabilitation and strengthening of unreinforced masonry has seen remarkable development on the basis of new techniques and materials [16-20]. The use of fibre reinforced polymers (FRPs), more specifically, present a number of advantages over traditional materials [19] due to their high tensile strength, low specific weight and excellent resistance against aggressive environmental actions. Usually, externally bonded FRP strips/sheets are adopted as a technique for strengthening shear masonry walls by increasing tensile capacity for supporting combined compression and shear actions under earthquakes.

In recent years, a Code of Practice for practitioners was edited to serve as a guideline for FRPs use [21]; it supplies formulas and suggestions. The strengthening of masonry walls with FRPs is opening new venues for experimental research centring on the possible performance of masonry subjected to cyclic loading [18].

The knowledge concerning the behaviour of structural masonry elements strengthened by FRPs continues to be insufficient even if many works [16, 20, 22] have investigated this strengthening technique main aspects. Adhesion between FRPs [23] and masonry with the dangerous mechanism of debonding or delamination still requires investigation [23-26]. The resistance of strengthened masonry walls in shear depends mostly on the bond of FRP strips/sheets to masonry surfaces and can limit conditions in design, especially, in the case of FRPs adhering to historic clay brick surfaces. Experimental and theoretical results have been presented in literature analysing the mechanisms of delamination between masonry walls [20] and FRPs [26-28] though behaviour was investigated on specimens under pull-out tests or on masonry walls having only one leaf. Unfortunately, multiple-leaf masonry walls strengthened with FRPs are rarely investigated regardless of the fact that many historic buildings were built using this very technique. In this paper the behaviour of double-leaf masonry wall models built with historic bricks in scale 1/3rd is experimentally studied in this paper. Wall models, both unreinforced and reinforced with FRPs, are analysed. Four wall models were subjected to in-plane cyclic loading; following shear damage with diagonal cracking, two wall models were strengthened using GFRP strips and one with steel fiber reinforced grout (SRG) strips, laid out diagonally, and bonded to only one of the surfaces of the wall. The behaviour of the wall models tested under in-plane cyclic loading is presented below and then discussed on the basis of the experimental results by analysing the different debonding mechanisms of the two types of composite materials used.

2. EXPERIMENTAL MODELS AND SET UP

A set of experimental tests were carried out on double-leaf historic brick wall models according to research works which have clearly shown that the strength of full scale in shear can be predicted through testing on small scale models [9,11]. Static tests were performed on four models, identified as M-LW1, M-LW2, M-LW3 and M-LW4, built with clay bricks in scale 1/3rd and obtained from full scale handmade bricks measuring 50 ÷ 60mm·150mm·300 mm obtained from the restoration of a historic XVIII century building from the Marche region in Italy. The masonry wall models were tested under combined compression and shear force. The choice of using double T shape sections (Figs. 1(a), and (b)) was dictated by the need to avoid bending cracking at the base of the wall model so that failure is initiated only due to shear [6, 20].

Static tests involved the unreinforced models, followed by two damaged specimens, M-LW1 and M-LW4, strengthened with GFRP strips and damaged specimen, M-LW3, strengthened with SRG strips. The wall models were built with two leaves of bricks placed in web position, detached by an intermediate layer of mortar and spaced out every two courses by units located in the stretcher position. The dimensions of tested models M-LW1, M-LW2, M-LW3 and M-LW4 are shown in Figure 1(a) and (b). The geometric choice adopted is justified by the intent of having a double leaf masonry wall with an organizational structure reflecting typical masonry used recurrently in historic buildings. The experimental models adopted are made up of two leaf masonry for the web, full masonry for flanges, an intermediate filler consisting of bits of brick and mortar, and linking bricks between the aforementioned leaves. Models M-LW1, M-LW2, M-LW3 and M-LW4 were made with bricks measuring approximately 100÷105mm·50mm·17mm. A cement: lime: sand (1:1:5) mortar by volume was used for the construction of the specimens. The sand grain size was three times smaller in order to reproduce actual mortar and friction at the interface of brick and mortar. A weak hydraulic mortar, cement: sand (1:3), was placed between the webs two masonry leaves. Brick specimens were taken from original historic clay bricks and tested under compression till failure. The test results showed remarkable uncertainty due to the type of clay. The average

compressive strength of the clay bricks was $f_b \approx 34.3$ N/mm^2. Three prismatic specimens measuring 40mm·40mm·160 mm were made in order to establish the strength of mortar, and flexural and compressive tests were performed. The mortar was characterized by the following average values of strength: compressive strength $f_m \approx 3.6$N/mm^2 and bending tensile strength $f_{mt}=1.61$ N/mm^2.

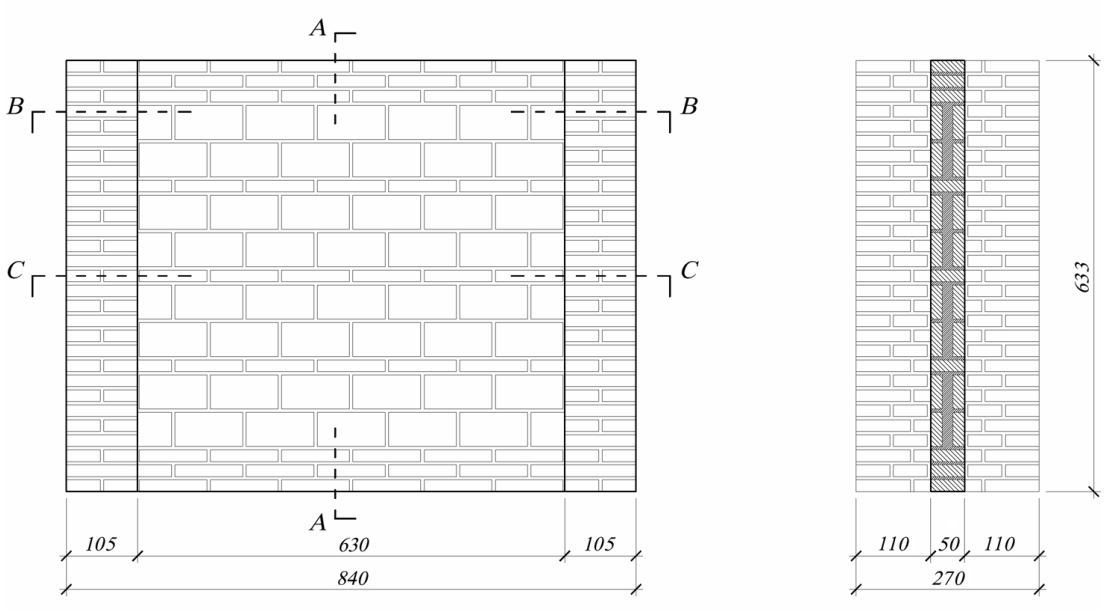

(a)

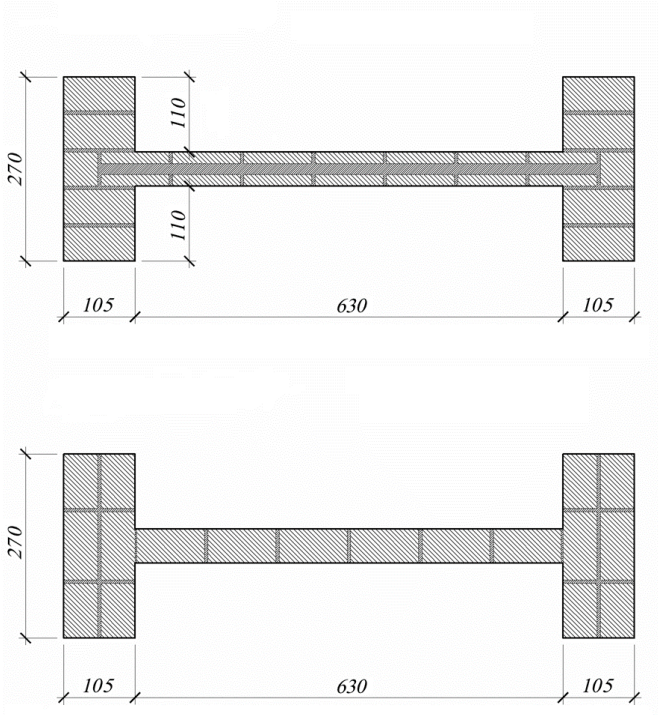

(b)

Figure 1. Dimensions of double-leaf brickwork model: (a) front view of model and vertical section; (b) horizontal sections.

A series of preliminary tests were done on small walls with clay bricks in scale to obtain the compressive strength f_y and f_x of masonry and Young's modulus of elasticity E_y, E_x in two orthogonal directions (Tab.1). The four models were built with full masonry for flanges and double-leaf masonry for web (Fig. 1). Flanges have the role of decreasing the maximum bending tensile stress and avoiding flexural cracking. Furthermore, flanges reduce the maximum value of shear stress distribution in the entire section, making its trend almost constant.

Table 1. Exp. mechanical values of masonry wallets by compression tests.

Direction of compressive load	Average Compressive Strength (N/mm^2)	Young's Modulus (N/mm^2)
Normal to bed mortar joint	f_y =13.5	E_y =8.76· 10^3
Parallel to bed mortar joint	f_x =10.4	E_x =6.90· 10^3

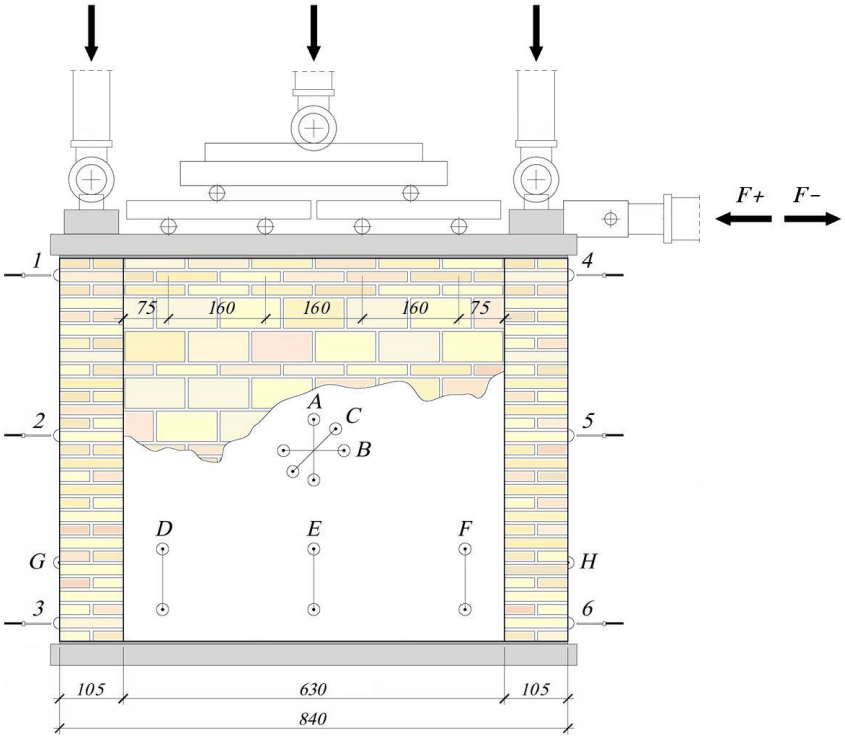

Figure 2 - (a) Set-up of exp. model of double-leaf brickwork walls with instruments: jacks to transmit vertical load and shear force; A,…,H bases to measure strain; LVDTs on the flanges.

The experimental compression and cyclic shear test set-up is shown in Figure 2. Vertical load was applied to the wall through a load distribution system by three hydraulic jacks (Enerpac type) to a steel plate placed on the top of the model. The steel plate, positioned on the top of the wall, was

attached to the panel with epoxy resin; it distributes both vertical load and horizontal cyclic load. The loads are applied using double phase jack over the entire panel. Bases to measure vertical strains were located at five positions along the length, labelled D, E, F on the web of the wall and by G, H on the flanges. Measuring bases were also used to evaluate principal strains in the centre of the wall; for this reason, Rosetta (A, B, C) were positioned in order to monitor the evolution of the wall's strains completely every cyclic load. The measurement of lateral deflection under horizontal cyclic load was achieved using inductive linear displacement transducers (LVTDs). LVTDs were applied on each flange in order to measure maximum displacement on top of the wall as well as its variation along the panel. The measurement of strain at the bottom of the wall allows analysing axial deformation, while the measurements carried out on the flanges highlight when they are subjected to tensile stress, because flanges face the bending effect of the load system applied.

3. RESULTS FROM TESTS ON UNREINFORCED MASONRY MODELS

Two models, M-LW1 and M-LW2, were tested in a first phase under combined vertical load and cyclic horizontal shear. Before the application of shear load, precompression was applied to both the web and the flanges of the wall by three vertical jacks (Fig. 2) and kept constant throughout the test; vertical force transmitted normal stress equal to σ_v =1N/mm^2. The cyclic shear load, F, was applied by horizontal jacks at stages till failure. Deflection and strain were also measured at various steps. Failure was sudden at horizontal forces value equal to about F_u=30kN and F_u= 36kN, respectively, for MLW1 and MLW2.

In Figure 3 the experimental diagrams of cyclic load, ± F, vs deflection, ± δ, at the top of the model wall (transducer no.1) is shown for M-LW1. The diagonal cracking distribution at the failure of both wall models M-LW1 is shown in Figure 4.

The behaviour of wall model M-LW2 under loading is summarized in the experimental diagrams of cyclic load, ± F, vs deflection, ± δ for transducers no. 4,5 and 6 positioned on one side of the panel (Fig. 5). Transducer no. 6 was applied close to the bottom of the model to control the fixed

constraint at the base of the model. Table 2 contains the main deflection values recorded for MLW2 for load cycle no. 6 up to ultimate load F= ±36kN.

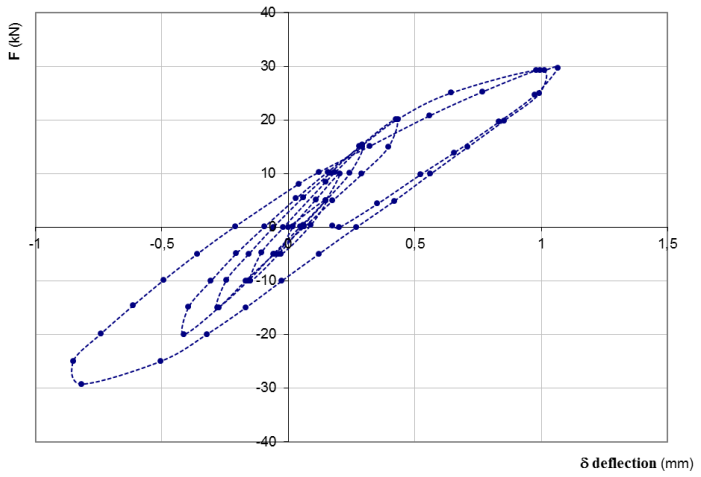

Figure 3 – Exp. cyclic horizontal load, F, vs deflection, δ, for unreinforced M-LW1- transd. no. 1

Figure 4 – Exp. cracking view of damaged model M-LW1.

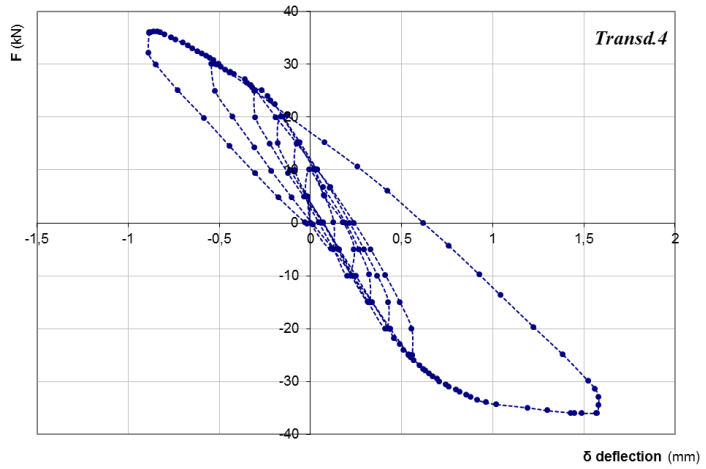

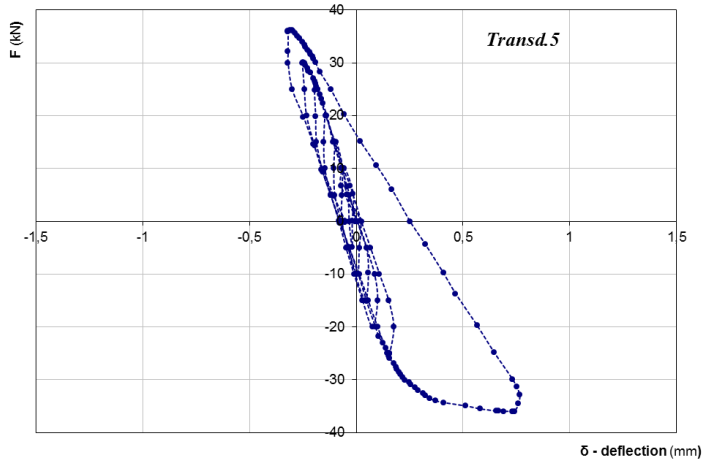

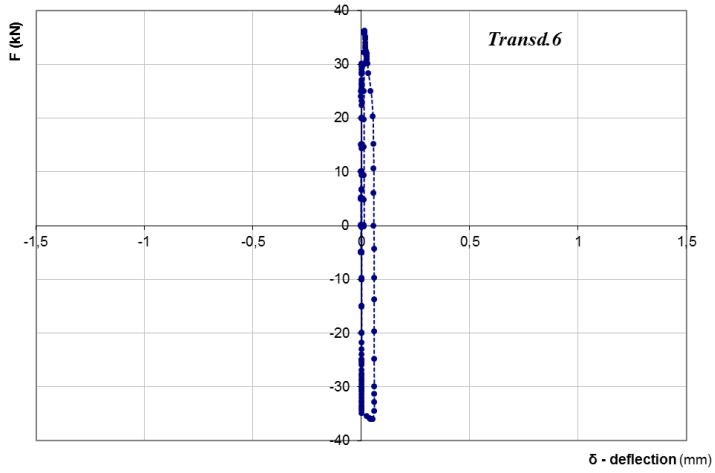

Figure 5 – Exp. cyclic horizontal load, F, vs deflection, δ, for unreinforced M-LW2 – transd. 4-5-6.

Table 2 – Main exp. values of deflection measured on LVDTs 1, …,6 for M-LW2.

Lateral Load **F** (kN)	**Cycle 6 - Load F = ± 36 kN - Deflection (**mm)					
	1	**2**	**3**	**4**	**5**	**6**
0.00	-0.05	-0.022	0.011	0.241	0.024	0.002
6.78	0.056	0.044	0.011	0.109	-0.029	0.001
10.01	0.109	0.075	0.013	0.038	-0.062	0.001
19.96	0.281	0.188	0.029	-0.188	-0.143	0.001
30.00	0.603	0.428	0.074	-0.544	-0.252	0.001
20.00	0.488	0.356	0.073	-0.425	-0.233	0.001
9.82	0.316	0.238	0.072	-0.213	-0.162	0.001
4.85	0.228	0.175	0.07	-0.103	-0.119	0.001
-0.34	0.131	0.109	0.062	0.016	-0.076	0.001
-10.01	-0.041	-0.003	0.039	0.231	0.014	0.001
-20.02	-0.213	-0.106	0.022	0.438	0.1	0.001
-30.03	-0.431	-0.231	0.003	0.709	0.228	0.001
-36.00	-1.081	-0.469	-0.019	1.575	0.742	0.053
-30.00	-1.038	-0.45	-0.076	1.525	0.733	0.06
-19.71	-0.797	-0.341	-0.066	1.225	0.566	0.059
-9.82	-0.566	-0.238	-0.048	0.928	0.409	0.059
0.00	-0.328	-0.128	-0.028	0.619	0.252	0.058
10.60	-0.047	0.019	-0.004	0.259	0.095	0.058
20.27	0.278	0.234	0.03	-0.125	-0.057	0.054
30.06	0.6	0.45	0.067	-0.503	-0.19	0.029
36.00	0.956	0.709	0.148	-0.884	-0.319	0.014
25.00	0.797	0.603	0.144	-0.725	-0.3	0.013
14.55	0.563	0.438	0.109	-0.444	-0.2	0.013
4.79	0.334	0.275	0.078	-0.175	-0.105	0.013
0.00	0.197	0.181	0.06	-0.016	-0.052	0.014

Figures 6 (a) and (b), contain the experimental diagrams of vertical deformation measured at the five points (G, H) on the lateral flanges and (D, E, F) on the web for the various load cycles for MLW2. Behavior appears to be substantially similar in both load directions for horizontal force ± F as far as concerns the deformations recorded at the base of model M-LW2. A comparison of cracking distribution between M-LW1 and M-LW2 is shown in Figures 7(a) and (b) with cracks prevalently located in the mortar joints with mainly diagonal directions.

The other two models, M-LW3 and M-LW4, were tested under the same in-plane loading by compression and cyclic shear force. Vertical precompression-normal stress was kept constant for these models with a value equal to σ_v =1.15 N/mm^2. Tests initially started imposing cyclic low load from F= ±1kN to ±5kN, and horizontal cyclic loads equal to F=±5kN were then applied.

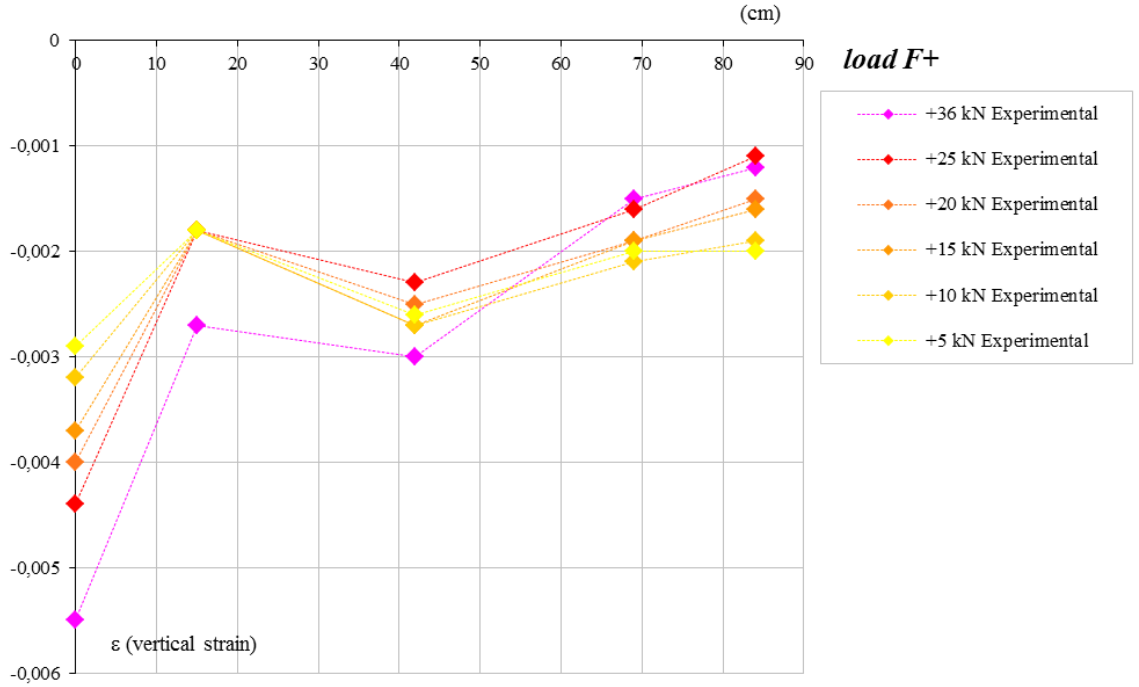
(cm)
load F+
+36 kN Experimental
+25 kN Experimental
+20 kN Experimental
+15 kN Experimental
+10 kN Experimental
+5 kN Experimental
ε (vertical strain)

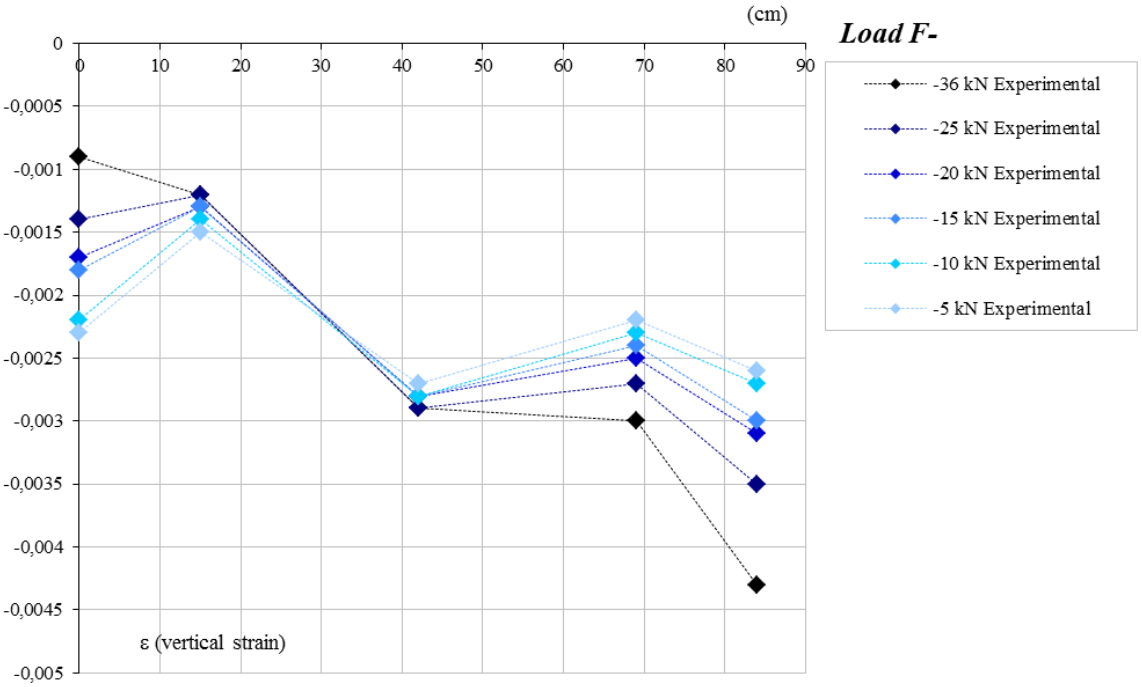
(cm)
Load F-
-36 kN Experimental
-25 kN Experimental
-20 kN Experimental
-15 kN Experimental
-10 kN Experimental
-5 kN Experimental
ε (vertical strain)

(a)

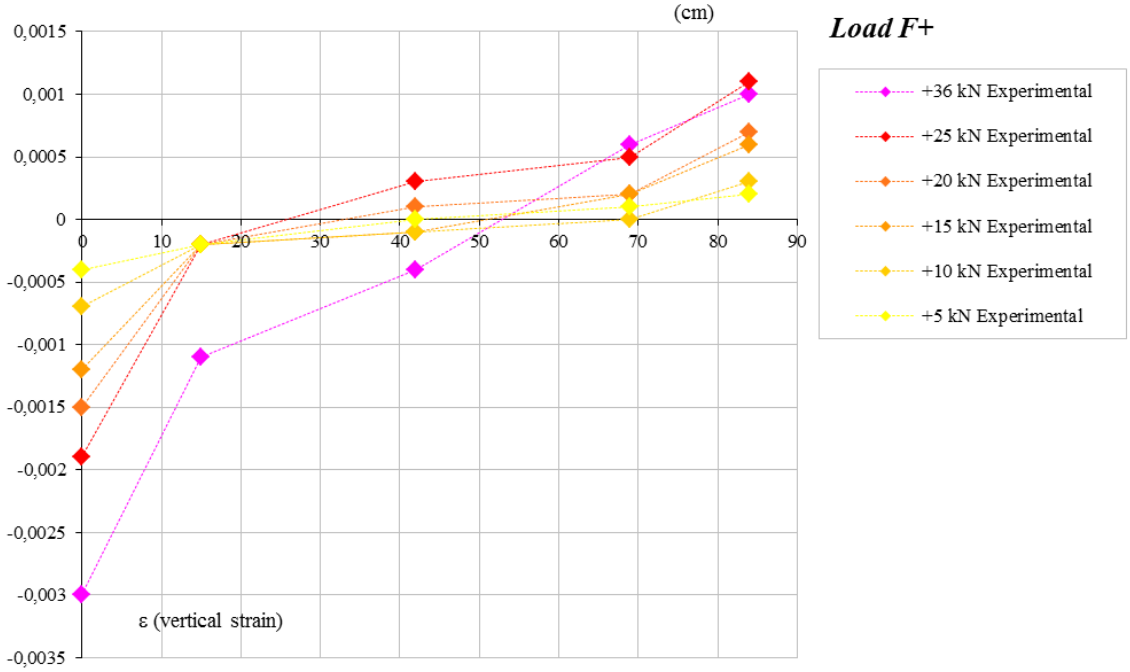

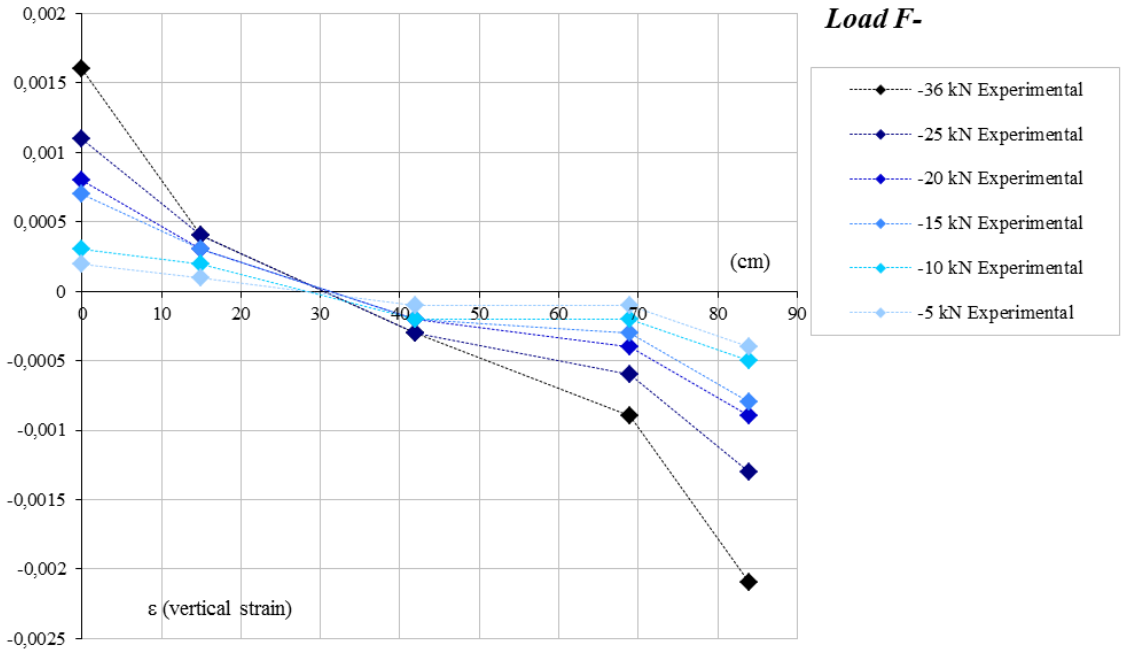

(b)

Figure 6 – Exp. diagrams vertical strains vs length for model M-LW2: (a) measured strains due to vertical loads plus horizontal load F^+ and F^-; (b) measured strains due bending for applied horizontal load F^+ and F^-.

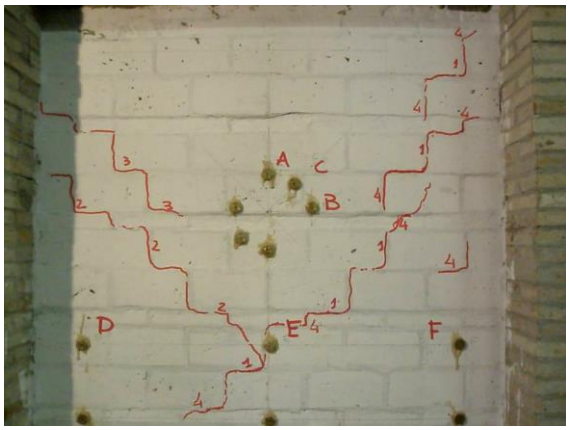

(a)

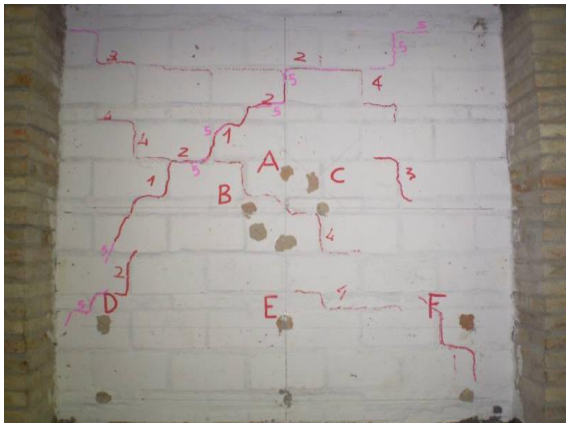

(b)

Figure 7 – Exp. cracking of tested models: (a) M-LW1 and (b) M-LW2.

In model M-LW3 the first cracks appeared when it was subjected to a horizontal load value equal to F=+10kN (Fig. 8). In model M-LW4 initial load cracking appeared at a value equal to F=-15kN marked number 1 (Fig. 10 (a)); the cracks appeared between the vertical mortar joints (Figs. 8 and 10) in both models.

Load increase was stopped at a horizontal shear value equal to F=+25kN for specimen M-LW3 (Fig. 9) and equal to F=-24kN for model M-LW4 (Fig. 11), because cracks appeared conspicuously with extended wall damage. They are marked by the number 8 (Figs. 8 and 10). Both models exhibit typical shear failure characterized by wide cracking between mortar joints and bricks with an angle of about $\pi/4$, typical of masonry walls subjected to seismic load and low normal stresses. Model M-LW4 definitely showed a cracking pattern more symmetrical than that of M-LW3, but the value of failure load was almost the same (Figs. 9 and 11).

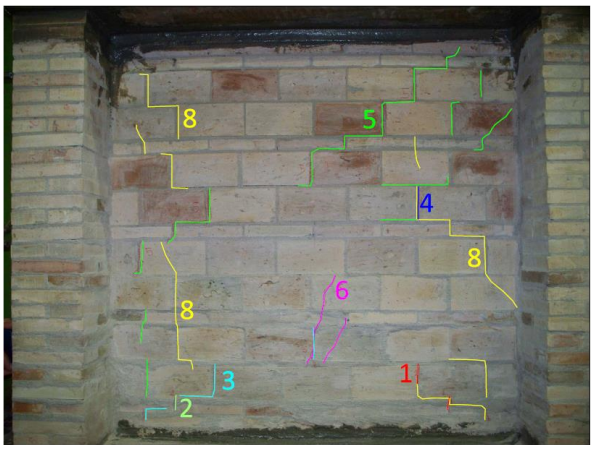

Figure 8 – View of exp. cracking of both façades for tested model M-LW3.

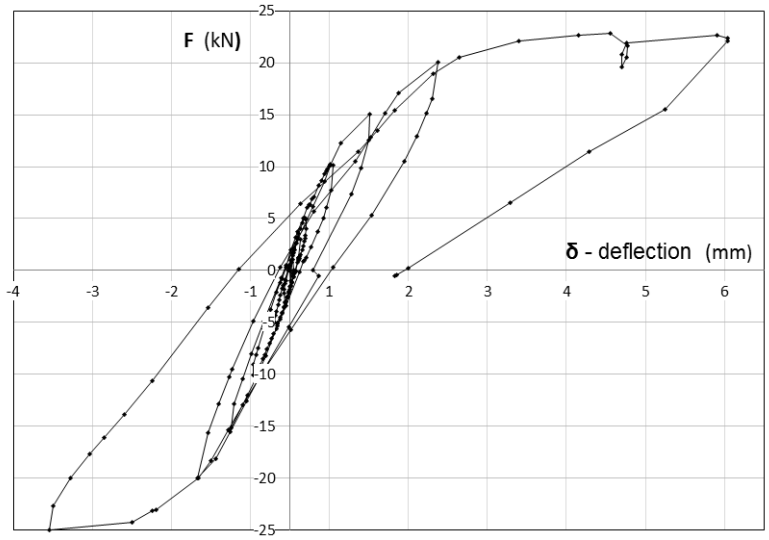

Figure 9 – Exp. diagrams load F vs deflection for model M-LW3 - measures at transd. 1.

The average ultimate shear stress, τ_{av}, referred to failure for the resistant area of the web, equal to about $32 \cdot 10^3 mm^2$ is indicated in Table 3. Figure 12 contains the experimental diagrams of average shear stress, τ_{av}, versus experimental horizontal deflection for the four tested models: M-LW1, M-LW2, M-LW3 and M-LW4.

Table 3 – Exp. average shear stress for unreinforced multiple-leaf wall models.

Unreinforced multiple-leaf wall models	Failure Lateral Load **F** (kN)	Average maximum shear stress τ_{av} (N/mm^2)	Type of cracking
M-L.W.1	29.30	0.94	shear failure
M-L.W.2	36.00	1.16	Shear failure
M-L.W.3	25.00	0.80	shear failure
M-L.W.4	24.00	0.78	shear failure

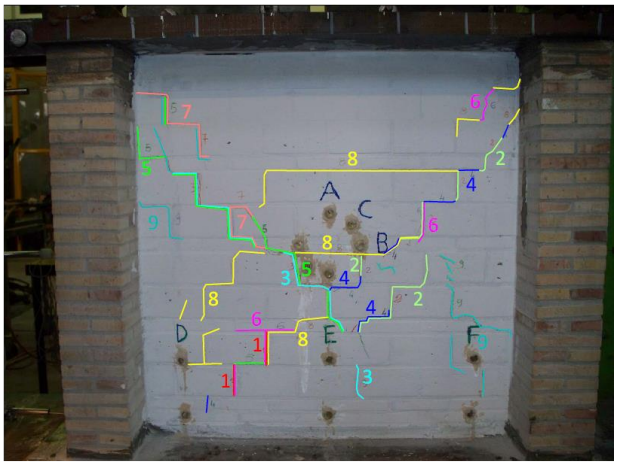

(a)

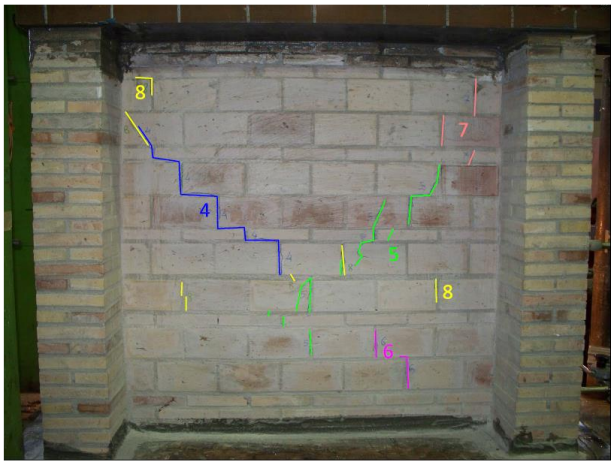

(b)

Figure 10 – Exp. cracking of tested model M-LW4: (a) first side and (b) second side of web.

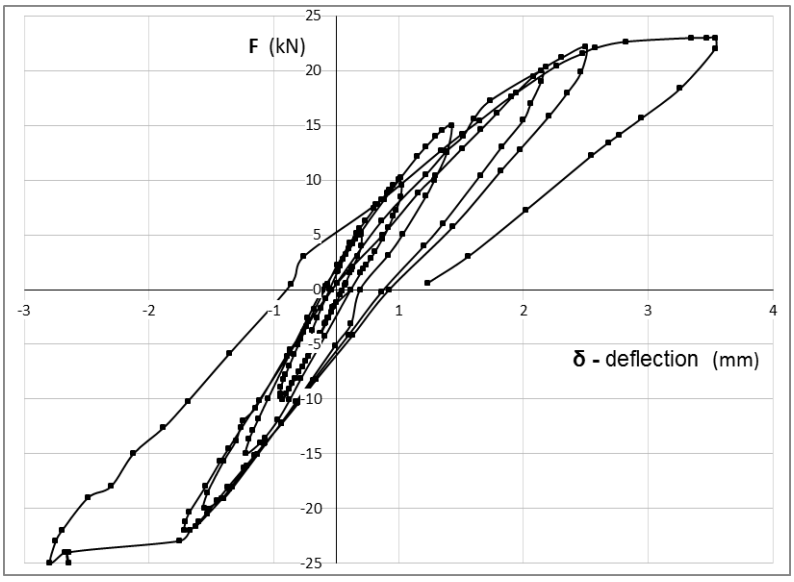

Figure 11 – Exp. diagrams load F vs deflection for model M-LW4 - measures at transd. 1.

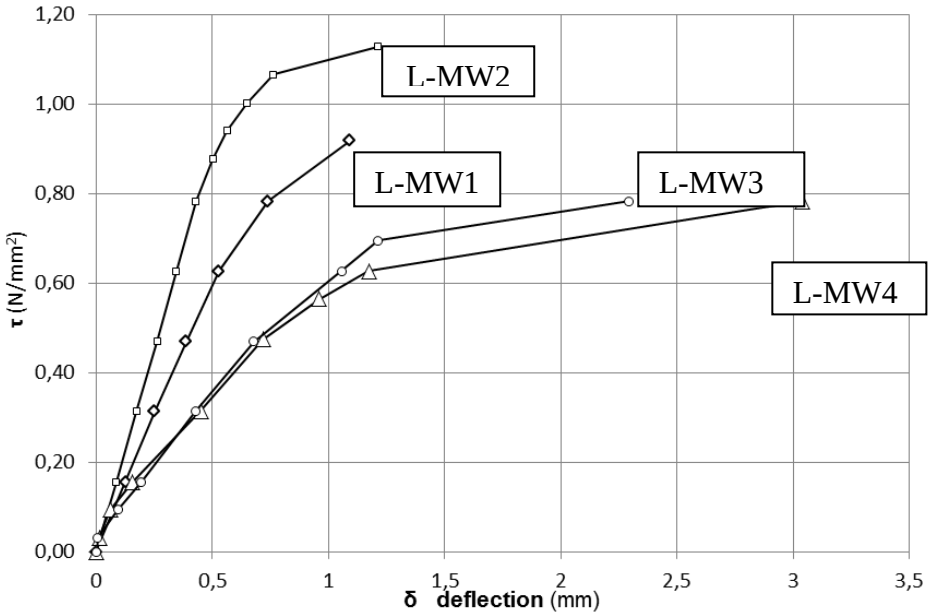

Figure 12 - Experimental diagrams average shear stress, τ_{av}, for resistant web area.

4. RESULTS FROM TESTS ON REINFORCED MASONRY MODELS

Similar experimental tests were carried out on damaged models after strengthening with external bonded CFRP and SRG strips. Previously, tensile tests were carried out on specimens of GFRP strips and steel reinforced polymer (SRP) strips [29]. Although SRG strips were adopted in the strengthening of the masonry wall model, tensile strength on SRP specimens permitted to control the strength capacity of this type of composite material with steel fiber. Both the glass and the steel fibers were soaked with epoxy resin as a polymer matrix offering high adhesion (such as Kimitech EP-IN), with a density of ρ=1,08g/cm^3. The main mechanical characteristics of epoxy resin are: maximum traction strength f_t > 30N/mm^2 and tensile Young's modulus equal to 1760N/mm^2. Tables 4 and 5 contain the experimental geometric data relative to the samples investigated and the experimental results obtained from traction tests according to ASTM D 3039 [29]. For the steel wires, the equivalent area was calculated considering the area and the number of wires in the specimens. Figure 13 shows the experimental failure of specimens by tensile tests with failure types.

Two damaged models, M-LW1 and M-LW4, were strengthened with diagonal GFRP strips applied on one face of the web; the damaged model, M-LW3, was strengthened with SRG strips.

Table 4 – Exp. dimensions of GFRP and SRP specimens.

Specimen	Composite Material	Equivalent Thickness - **t** [mm]	Measured thickness [mm]	Width - **b** [mm]	Area A_f [mm^2]	Equivalent Area $\mathbf{A_{fib}}$ [mm^2]
TG1	**GFRP**[1]	0.12	1.17	14.38	16.82	5.18
TG2	**GFRP**[1]	0.12	1.22	15.12	18.45	5.44
TA1	**SRP**[2]	0.48	3.30	21.04	69.43	4.81
TA2	**SRP**[2]	0.48	3.10	19.24	59.64	4.33

1. FIDGLASS UNI 300 HT 73

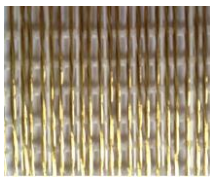

2. FIDSTEEL 3x2-4-12-500 HARDWIRE

Table 5 - Exp. results by tensile tests on GFRP and SRP specimens.

Specimen	Composite Material	Maximum Load $\mathbf{F^{max}}$ [N]	Normal stress $\boldsymbol{\sigma_f}$ [N/mm²]	Equivalent strength $\boldsymbol{\sigma_{fib}}$ [N/mm²]	Ultimate strain* $\boldsymbol{\varepsilon_{FRP}}$ (%)	Density* $\boldsymbol{\rho}$ (g/m^2)	Young's Modulus $\mathbf{E_f}$ [GPa]	Equivalent Modulus $\mathbf{E_{fib}}$ [GPa]	Type of failure
TG1	GFRP	6365	378.3	1229.5	2.00	300	-	-	AGM
TG2	GFRP	7169	388.6	1317.1	2.00	300	19.0	64.0	AGM
TA1	SRP	16910	243.5	3515.6	1.60	-			LGM
TA2	SRP	14267	239.2	3295.7	1.60	-	15.5	213.8	LGM

[*] values declared by the manufacturer.

(a)

(b)

Figure 13- View of experimental failure by tensile tests: (a) GFRP specimen – failure type AGM (Angled, Gage, Middle); (b) SRP specimen – failure type LGM (Lateral, Gage, Middle).

The aims of the experiment were centred on the system's crisis mode; the system being composed of masonry plus strengthening. In general, the following failure mechanisms apply: failure of the masonry due to normal traction stress or shear; failure due to crushing of the masonry; loss of adhesion of the strengthening on the masonry, failure of the same strengthening.

The material used to strengthen models M-LW1 and M-LW4 is a composite characterized by high resistance; the glass fibres are mainly made up of silica (SiO_2) in tetrahedral structure (SiO_4) with aluminum oxides and metallic ions in various proportions in order to facilitate working operations. An epoxy resin was adopted in the matrix.

Disadvantages of glass-fiber polymer composites are represented by the vastness of the temperature range for operating limited by the glass transition temperature, by their moderate fracture toughness and their sensitivity to moisture when applied to wall structures Strengthening with SRG strips is based on the adherence of the same cement material which represents the steel wires' driving force.

The adhesion of the strengthening plays an important role in the oversell efficiency of the system and it will be further analysed by comparing the results obtained using the two types of composites. It is well known that the loss of resistance of the FRP-masonry joint system can occur in various conditions: in proximity of the surface where the composite comes into contact with the mortar material, involving a superficial film of the wall surface; along the contact surface of the wall material and the adhesive; at contact between the thin layer of adhesive and the composite and finally, inside the same composite for interlaminate failure. Generally, resistance to traction-shear of the adhesive layer is higher so that collapse of the joint occurs due to the detachment of a part of the sublayer which remains on the FRP [25].

4.1. Wall models with GFRP strips

Three diagonal GFRP strips with an inclination of $\pm\pi/4$ were adopted as strengthening in M-LW1 and M-LW4, with a width value equal to 30mm (Fig. 14). Applying the strengthening entailed a series of operations: preparing the support by eliminating any surface impurity in the masonry; applying a *primer* obtained by mixing two components; applying a layer of adhesive and, finally, a GFRP composite. The thickness of the GFRP strips was equal about to 1.5mm.

In addition to all the instruments used for the test on the unreinforced models, two strain gauges on M-LW1 and six strain gauges on M-LW4 (Fig. 14 (a)) were also used in order to measure strain

along the reinforced strips. The tests were carried out with the same procedures adopted for the test on the unreinforced walls: horizontal shear force was applied with increasing intensity cycles with an increase of ±5kN for each cycle.

(a)

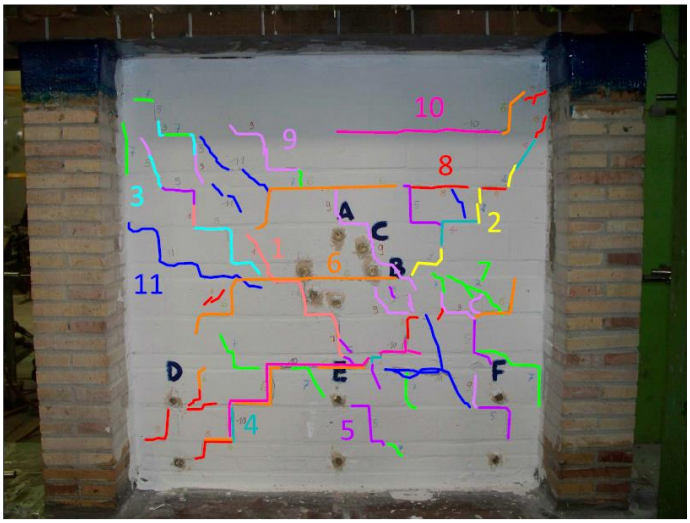

(b)

Figure 14 – (a)Reinforced model M-LW4 by GFRP strips with 6 strain gauges on central diagonal strips; (b) view of cracking distribution on one side without strengthening.

The experimental diagram cyclic horizontal load, F, versus deflection, δ, recorded for M-LW1 model is shown in Figure 15 for transducer no. 1 at the top of wall. Failure occurs at a horizontal load value equal to approximately F=-21kN.

The evolution of the cracking trend for M-LW1 observed during the test is contained in Figure 16 for the side without strengthening. Cracking begins at horizontal force approximately F=-10kN; for F=-20 kN, cracks numbered 5 are highlighted and the onset of the strengthening debonding is also

highlighted. Subsequently for horizontal force, F=+20 kN, cracks 6 and 7 formed. The cracks occurred at the mortar-brick interface and showed a prevalently diagonal trend which indicates that the crisis occurred because the shear resistance of the masonry wall was exceeded. Sliding of the joints was also recorded. In this case, the ultimate strength of L-MW1 is not increased compared to unreinforced model L-MW1, although relevant differences between experimental diagrams horizontal load versus deflection are recorded.

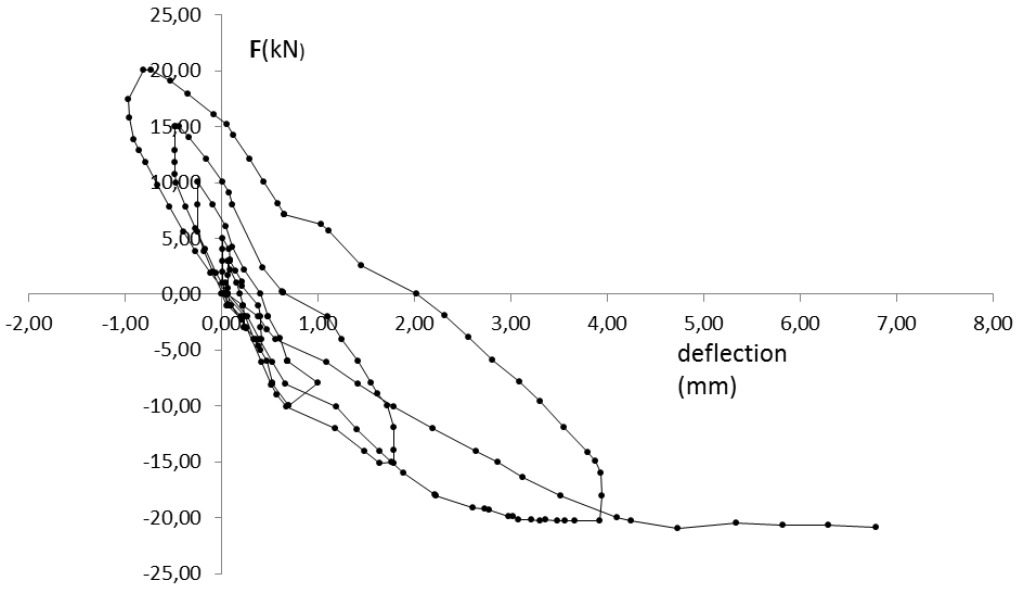

Figure 15 – Exp. cyclic diagram horizontal load, F, vs deflection, δ, at the top of wall model for reinforced L-MW1.

Figure 16 – Side view of cracking of reinforced model M-LW1 at horizontal load F≈±21kN.

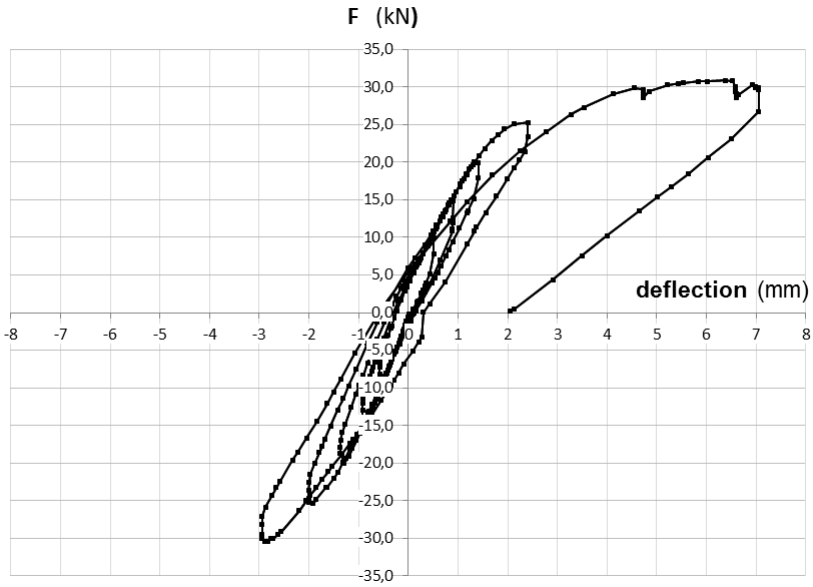

Figure 17 - Reinforced model M-LW4 by diagonal strips Glass-FRP with six strain gauges to measure strains under tests.

The experimental diagram cyclic horizontal load, F, versus deflection, δ, recorded for M-LW4 model is shown in Figure 17 for transducer no. 1 at the top of wall. Following the test vast cracking is observed, as shown in Figure 14(b). The first cracks were registered at F=+15kN; corresponding to load F=-18 kN cracks 2 and for F=+18 kN type 3 cracks. At load cycle F=±28 kN crack types 8 and 9 were registered. Reaching F= -30 kN cracks 10 and 11 are registered.

Table 6 – Strain measures at positions 1,…,6 on diagonal GFRP strips M-LW4.

Load cycle Lateral Load **F** (kN)		Values measures on strain gauges (10^{-6})					
		1	**2**	**3**	**4**	**5**	**6**
F=± 10	-5.0	-53.6	-42.7	-41.0	89.1	53.0	61.0
	-10.0	-105.5	-83.2	-93.0	139.3	89.4	122.2
	-5.0	-57.7	-51.2	-56.5	94.6	54.8	85.5
	0.0	0.4	-9.0	-15.4	35.4	9.7	34.3
	5.0	56.0	36.5	36.3	-38.5	-46.2	-28.1
	10.0	98.1	80.8	101.0	-120.6	-105.2	-94.0
	5.0	63.7	51.1	59.3	-58.8	-63.1	-47.3
	0.0	5.0	-0.6	-1.6	35.8	5.2	20.0
F=± 20	-10.0	-101.0	-87.5	-105.0	175.8	93.7	153.0
	-20.0	-218.6	-176.0	-242.6	220.0	136.1	283.1
	-10.0	-81.0	-85.0	-142.2	134.9	64.4	172.9
	0.0	40.0	5.3	-48.0	48.1	-1.9	61.3
	10.0	140.5	108.0	110.7	-136.1	-135.8	-93.4
	20.0	169.1	148.5	271.0	-304.2	-262.0	-217.7
	10.0	110.0	92.8	126.6	-130.0	-131.6	-70.5
	0.0	26.1	12.2	-4.7	67.8	8.8	41.6

F=± 30	-10.0	-95.2	-104.0	53.8	179.4	108.6	83.5
	-20.0	-238.5	-215.0	-273.8	213.8	162.2	329.5
	-30.0	-514.0	-264.6	-453.7	194.0	203.8	649.7
	-20.0	-259.7	-140.2	-275.1	191.3	180.0	494.3
	-10.0	-51.2	-82.7	-150.0	161.0	135.6	269.7
	0.0	92.3	-4.0	-34.0	52.5	41.7	103.7
	10.0	240.4	134.0	394.4	-344.0	-228.6	-153.3
	20.0	254.4	176.3	1433.0	-663.6	-416.3	-340.5
	30.0	282.4	324.2	4360.6	-941.0	-536.4	-591.3
	20.0	260.1	313.2	4360.5	-834.0	-772.3	-421.7
	10.0	218.4	224.0	2556.1	-511.0	-578.4	-180.2
	0.0	95.5	68.1	790.0	-76.0	-294.0	-72.0

Six strain gauges were applied for this test; the values measured permit recording that at load F=+30kN, extensimeter no. 3 registered (Tab. 6) a meaningful increase of deformation (Fig. 18). It is worth pointing out that the forces having a positive sign (Fig. 2) cause traction deformation in the group of extensometers numbered 1, 2 and 3; on the other hand, those with a negative sign induce traction deformation for extensometers 4, 5 and 6. In the direction of the negative sign force, F^-, we have the diagrams registered for extensometers 6, 5 and 4 contained in Figure 19. In extensometer no. 6 particularly high values are registered when force F=-30kN is exceeded up to failure of the GFRP strengthening strips for load F=-33kN.

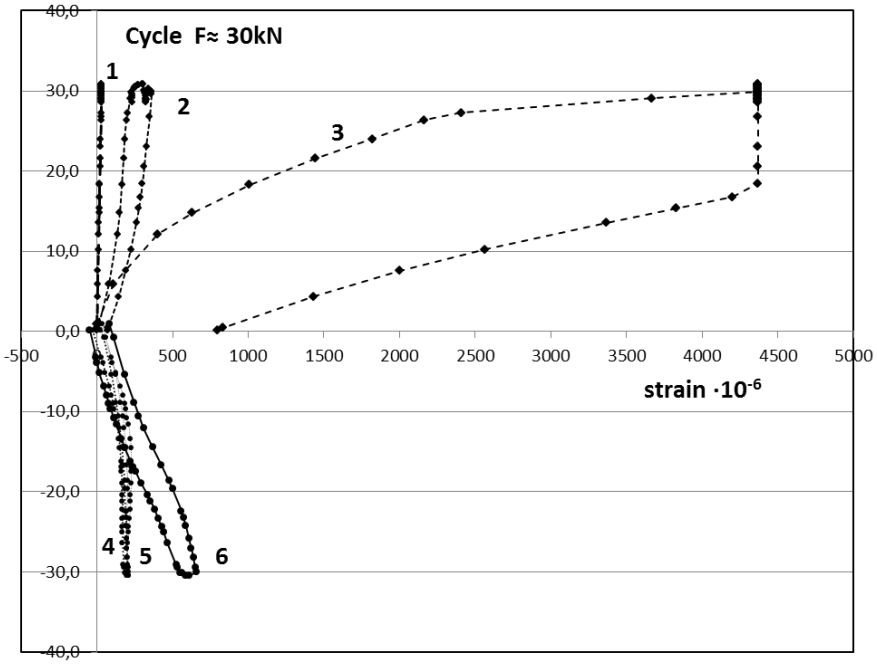

Figure 18 - Exp. diagrams of horizontal load F vs strain measures on strain gauges no. 1,…,6 on GFRP strips - reinforced model M-LW4 under loading cycle F≈±30kN.

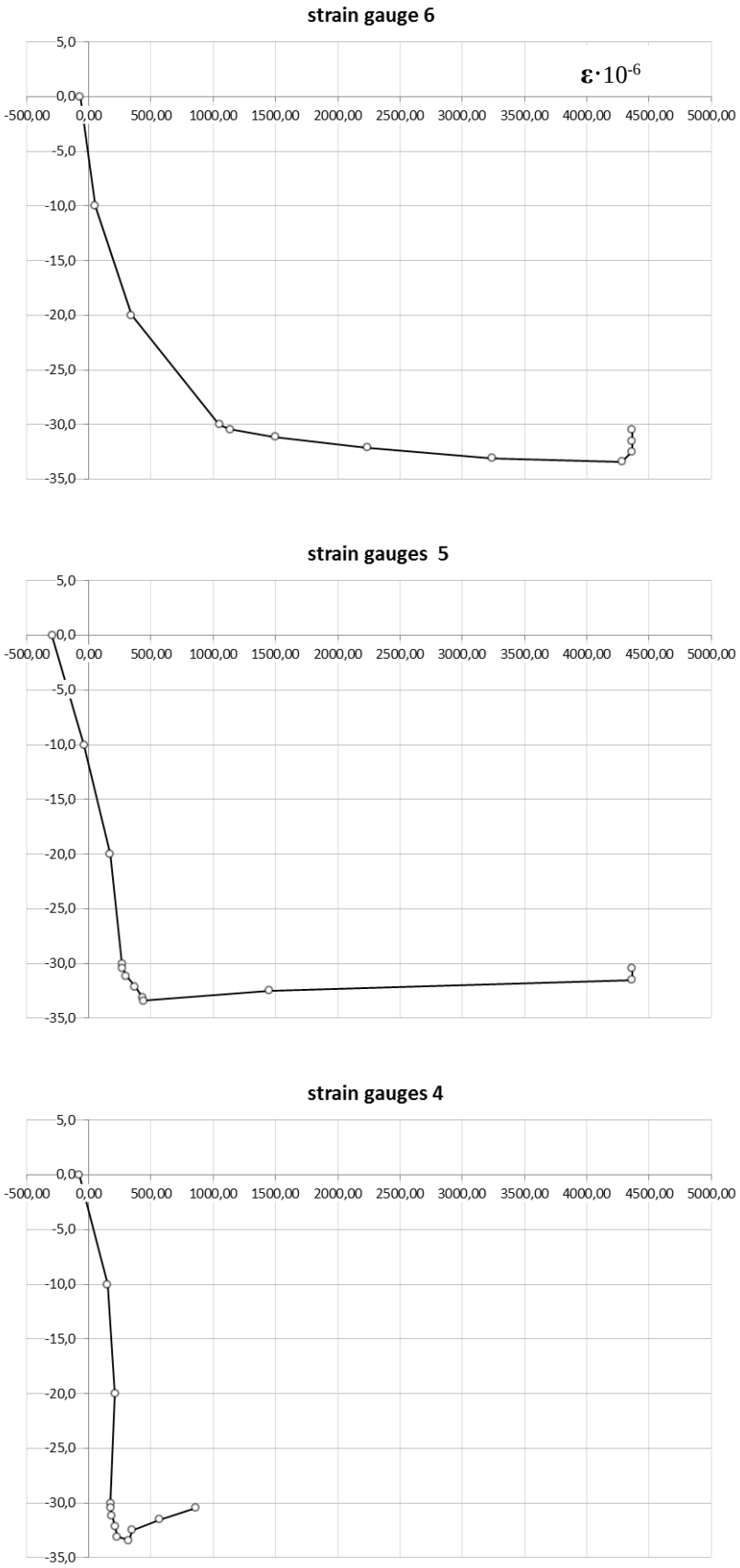

Figure 19 – Exp. diagrams of horizontal load F vs strain measures ($\cdot 10^{-6}$) on strain gauges no. 4,5,6 on GFRP strips in reinforced model M-LW4.

4.2. Wall model with GFRP strips

One specimen, MLW3, was reinforced with SRG strips always only on one side. The strengthening system is based on the use of principal materials in *unidirectional steel fibres* (UHTSS Hardwire® 3x2x4-12-500) low density type (1.57 wires/cm) and mortar, suitable for Kimisteel LM type surface operations, mixed with two component epoxy resin.

The width of the single SRG strip in the strengthening is equal 70mm (Fig. 20(a)); the thickness of the mortar strengthening applied is approximately 3.5mm.

The instruments used for tests on model M-LW3 were the same as those used in the previous shear tests on the reinforced panels: five LVTDs no. 1,…4, 5 placed on the flange (Fig. 21) allowed registering the lateral deflection values; six strain gauges applied (Fig. 20(b)) along the two principal diagonals of the strengthening to measure deformation on the strengthening. The panel was subjected to a vertical precompression load equal to $\sigma_v = 1.15$ N/mm^2.

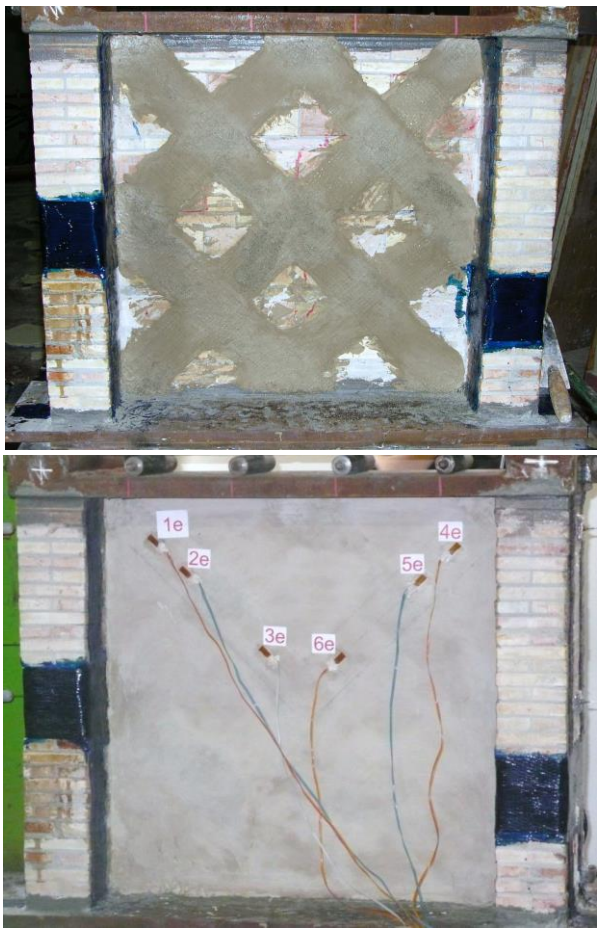

(a) (b)

Figure 20 - Experimental reinforced model M-LW3 with (a) diagonal SRG strips and (b) location of strain gauges glued on central diagonal strips 1,2,3 and 4,5,6.

Figure 21 – Exp. reinforced model M-LW3 and position of transd. 1,..,6.

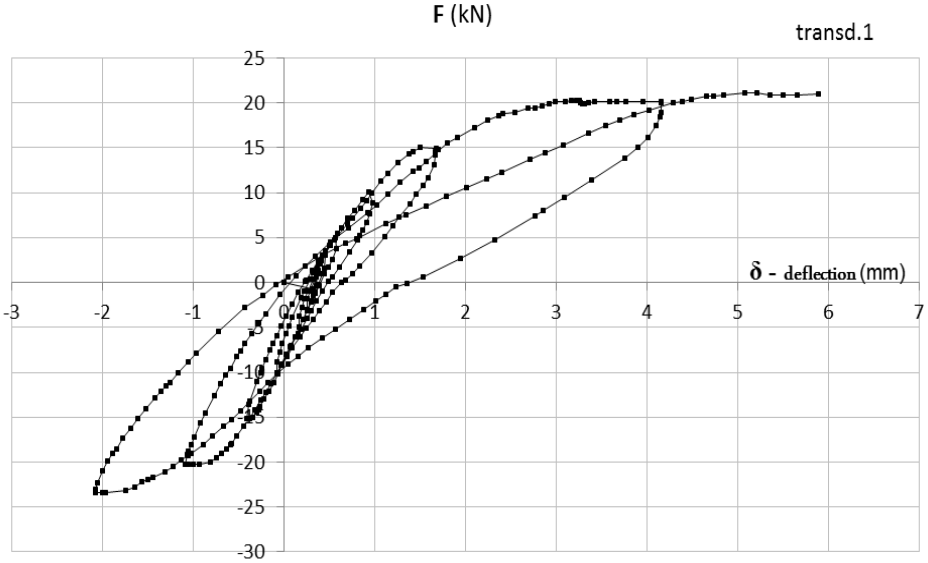

(a)

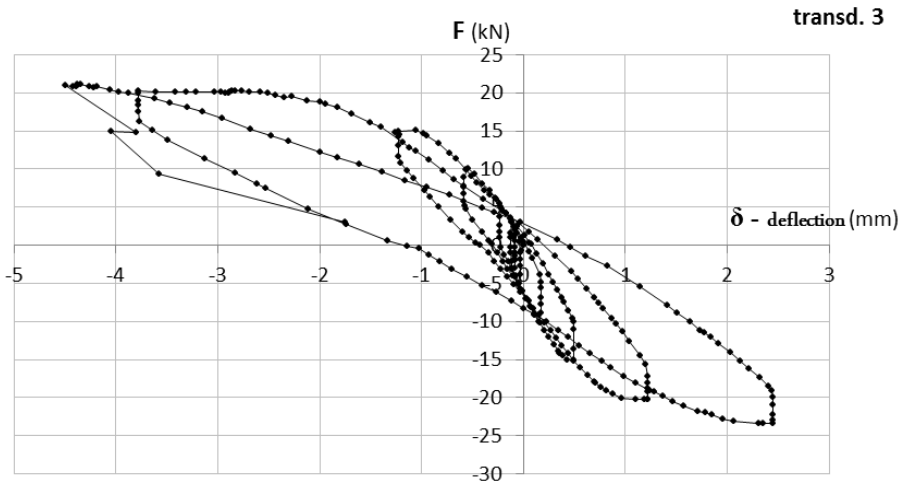

(b)

Figure 22 – Exp. diagrams cycles load, F, vs deflection for transducers: (a) no.1 and (b) no.3 in reinforced model M-LW3 with SRG strips.

The experimental diagrams for cyclic horizontal load, F, versus deflection, δ, recorded for M-LW3 model are shown in Figure 22(a) and (b), respectively, for transducer no. 1 and 3 at the top of model. Figure 23 contains a view of cracking for one side of M-LW3 without strengthening.

Experimental diagrams horizontal load, F, versus strain measures, ε_{SRG}, on strain gauges 1,2 and 3 are shown in Figure 24.

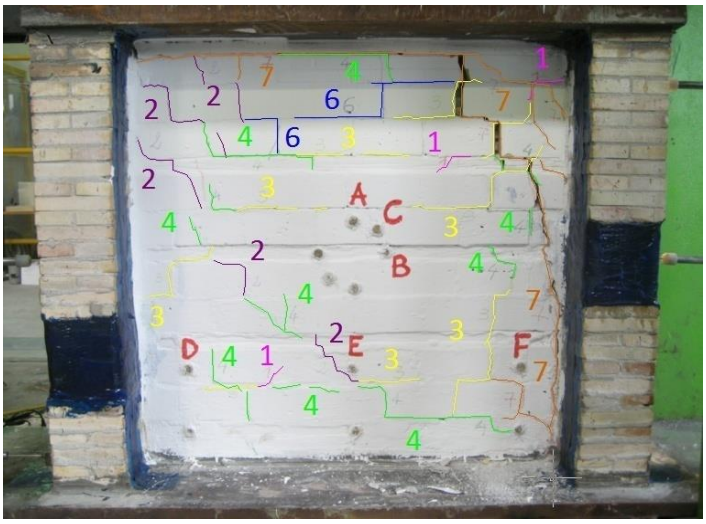

Figure 23 –View of cracking on one side of exp. reinforced model M-LW3 at failure.

The test was carried out as follows: the first load horizontal cycles were obtained for reduced horizontal strain values: F=±1kN÷5 kN; subsequently proceeding to step ±5 kN. At value F=+15kN type 2 cracks appeared 2 (Fig. 23), while type 3 cracks appeared at F=-20 kN. At the same value of F=-20 kN, on the reinforced side of the model core in strain gauges 3, 2 and 1, prone to deformation by compression, an increase in horizontal load deformation can be noted with *buckling* of the SRG strip on the principal compressed diagonal.

At value F=+20 kN, type 4 cracking was observed, while evident debonding with cracking of the cement matrix was observed on the side of the strengthened core, corresponding to the position of strain gauge no. 6 (Fig. 29(b)). Finally, the maximum resistance capacity recorded for model M-LW3 was equal to F=-23kN.

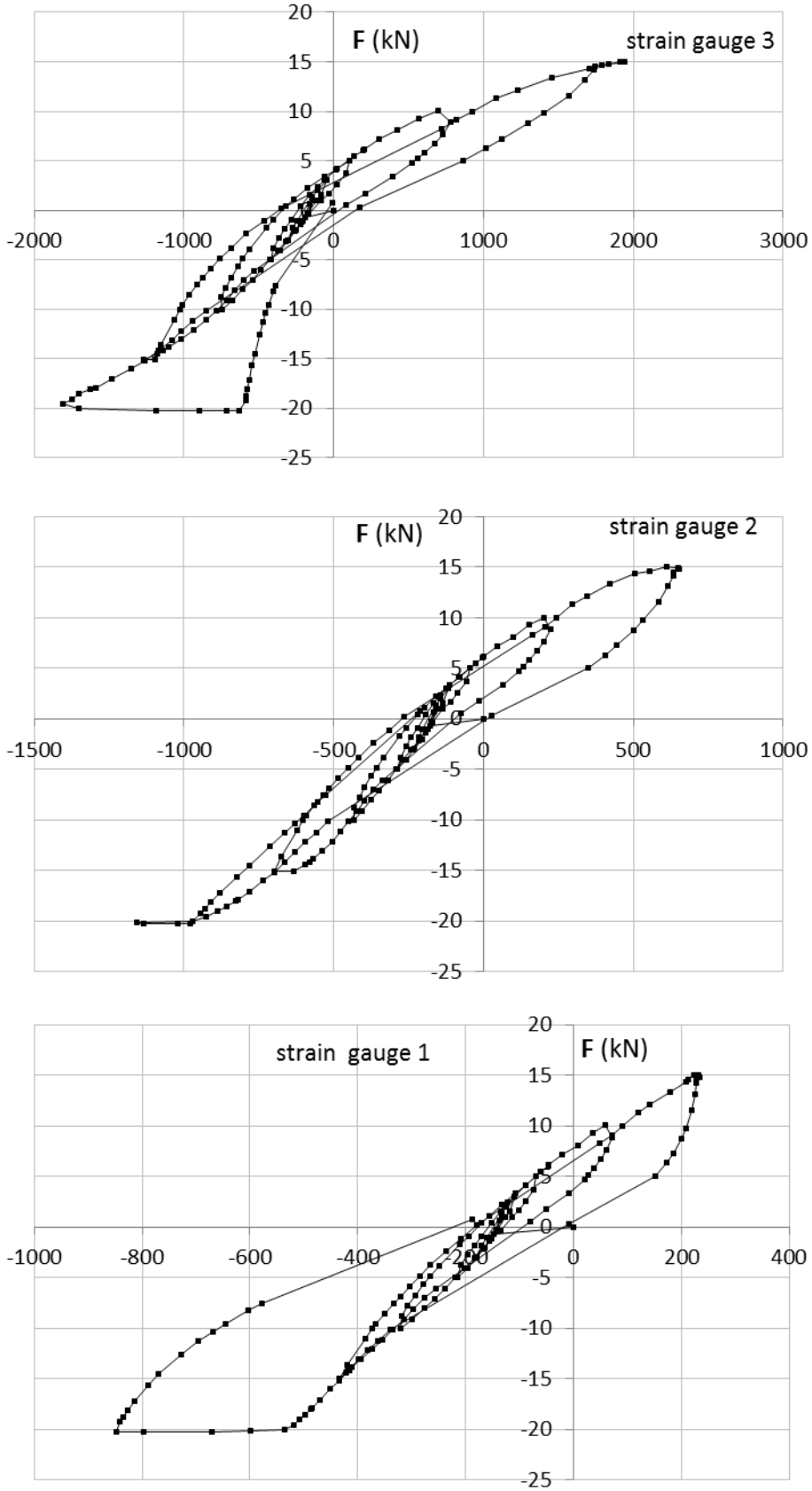

Figure 24 - Experimental diagrams load, F, vs strain values $\varepsilon \cdot 10^{-6}$ measured on strain gauges glued to diagonal SRG strip for reinforced M-LW3.

5. COMPARISON OF RESULTS AND DISCUSSION

The experimental tests carried out on models MLW1,…, MLW4 – both reinforced and unreinforced - allowed to record a vast number of data that require detailed analysis. The unreinforced panels, characterized for having a double leaf web and subjected to a combined compression and shear load condition, maintained their behaviour without a separation of the two leaves up to shear failure. Although models MLW1,…, MLW4 do not present the same ultimate resistance to shear value (Tab. 3), damage mechanism with cracking in the mortar joints is comparable among the various models.

A comparison between the responses of unreinforced models and models reinforced with GFRP strips, shown in Figures 25 and 26, respectively, for M-LW1 and M-LW2, was done with the experimental cyclic diagrams horizontal load, F, versus deflection, δ, at LVDT no. 1 located on the top of the models. It may be noted that the strength of the damaged wall model with GFRP strips increased with the ultimate deflection with an energy dissipation capacity higher than that of the unreinforced wall model.

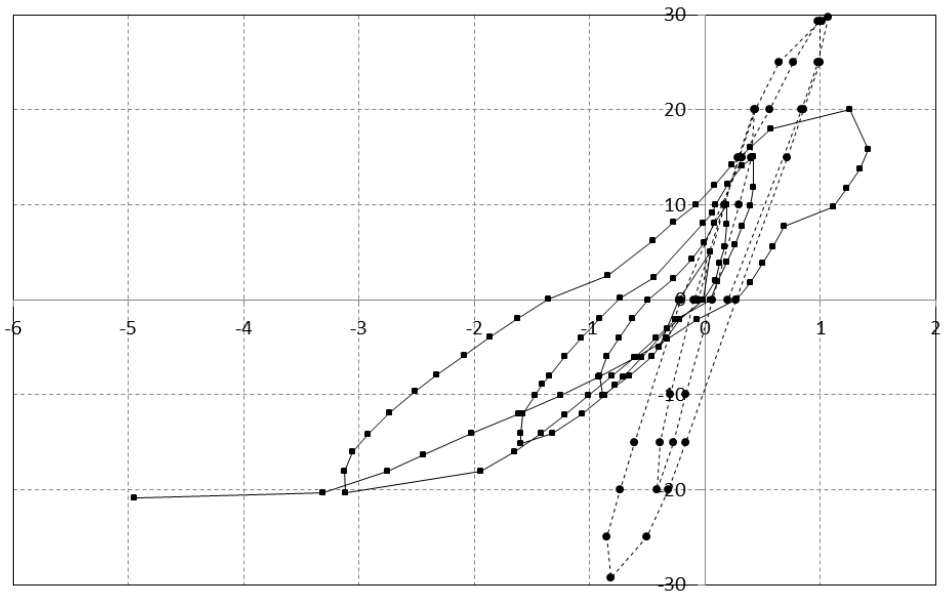

Figure 25 – Comparison of exp. cyclic diagrams load, F, vs deflection, δ, at point of transd. no. 1 for unreinforced (dashed line) and reinforced (continuous line) M-LW1 with GFRP strips.

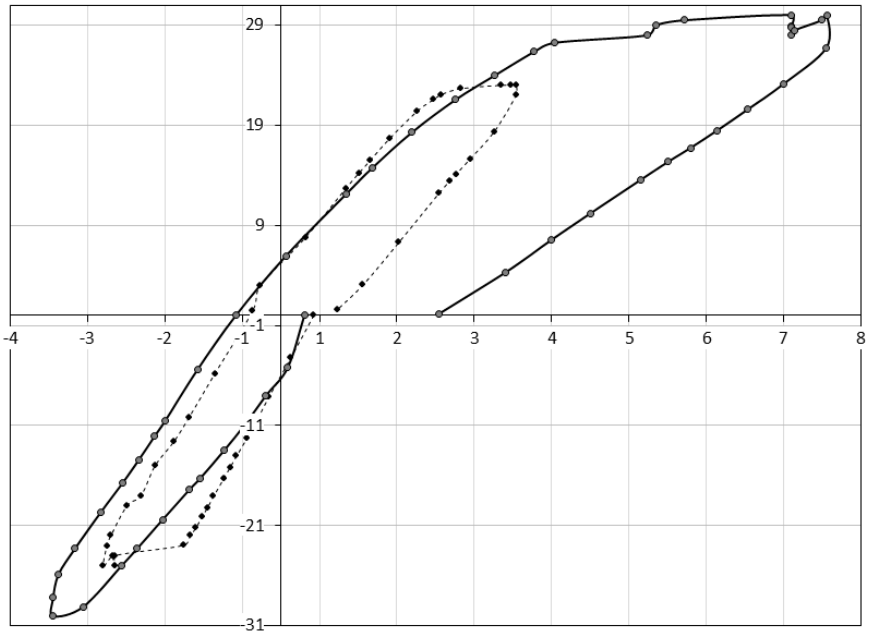

Figure 26 – Comparison of experimental cyclic diagrams horizontal load, F, vs deflection, δ, transd. no. 1 for unreinforced (dashed line) and reinforced (continuous line) M-LW4 with GFRP strip.

In Figure 27 a comparison is shown for M-LW3, unreinforced and strengthened with SRG strips. In this case also the strengthening allows to increase deflection although ultimate lateral force does not increase as it does for model M-LW1 strengthened with GFRP strips. So that the advantage of strengthening in this type of double-leaf masonry is higher ductility with better energy dissipation capacity.

Failure of the three strengthened models manifested with cracking of the masonry and with different debonding mechanisms for the two types of GFRP/SRG strengthening adopted. In the case of strengthening with GFRP strips, debonding of the diagonal strips occurs due to traction equal to $\varepsilon = 2500 \div 3000 \cdot 10^{-6}$ (Fig. 28).

In the case of SRG strips, the debonding mechanism is principally due to deformations due to compression with phenomenon such as buckling of the steel wires (Fig. 29(a) and (b)). Figure 30 shows a comparison between the values recorded for deformations by strain gauges 1, 2 and 3 in model M-LW3. It can be noted how, at same horizontal force F, higher deformation values are recorded for the forces that induce compression in the principal diagonal SRG strip, resulting from the instability of the steel wires.

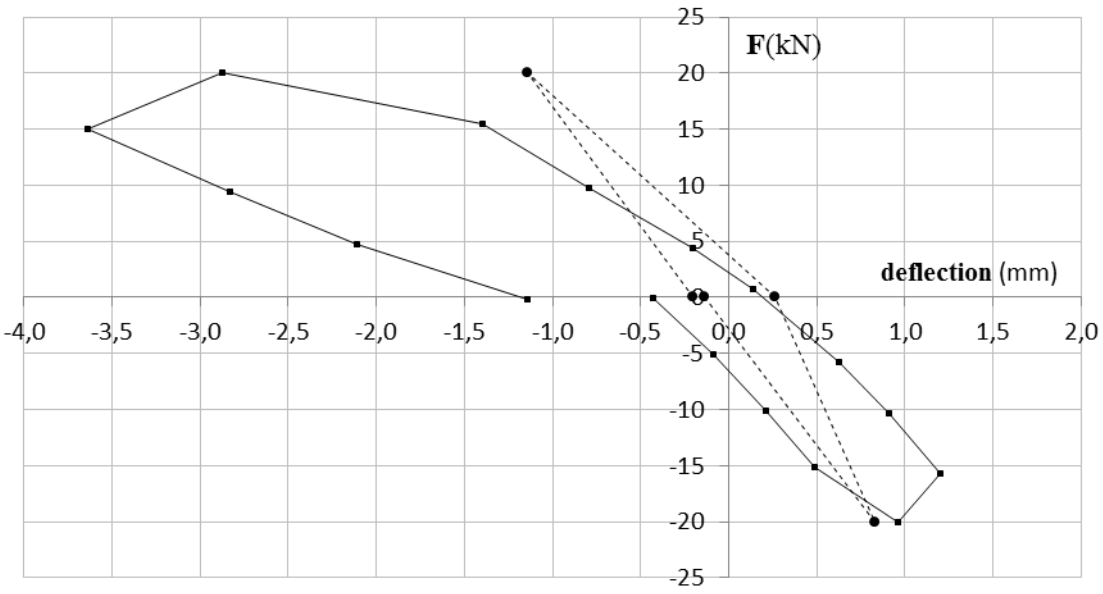

Figure 27– Comparison of exp. cyclic diagrams load, F, vs deflection, transd. no. 1 for unreinforced (dashed line) and reinforced (continuous line) L-MW3 with SRG strips - at cycle 20kN.

(a)

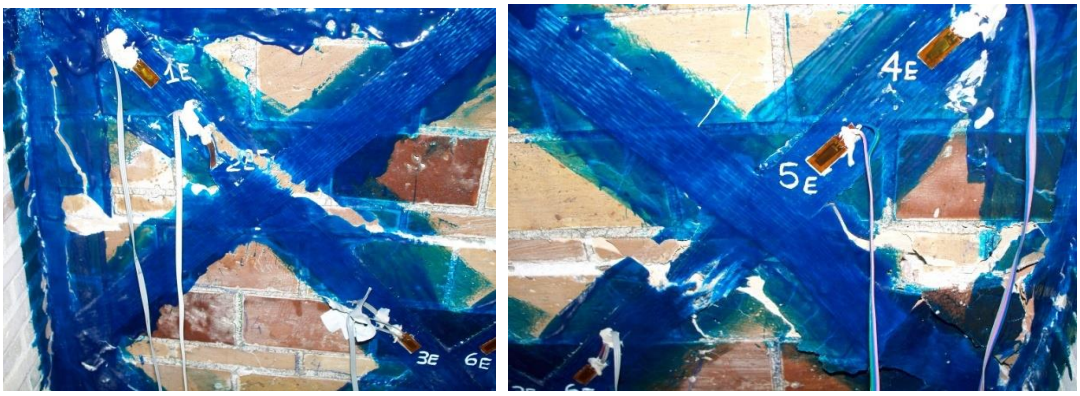

(b)

Figure 28 - View of failure of GFRP strips on strengthened M-LW1 and M-LW4: (a) debonding of strips; (b) tensile failure of strips.

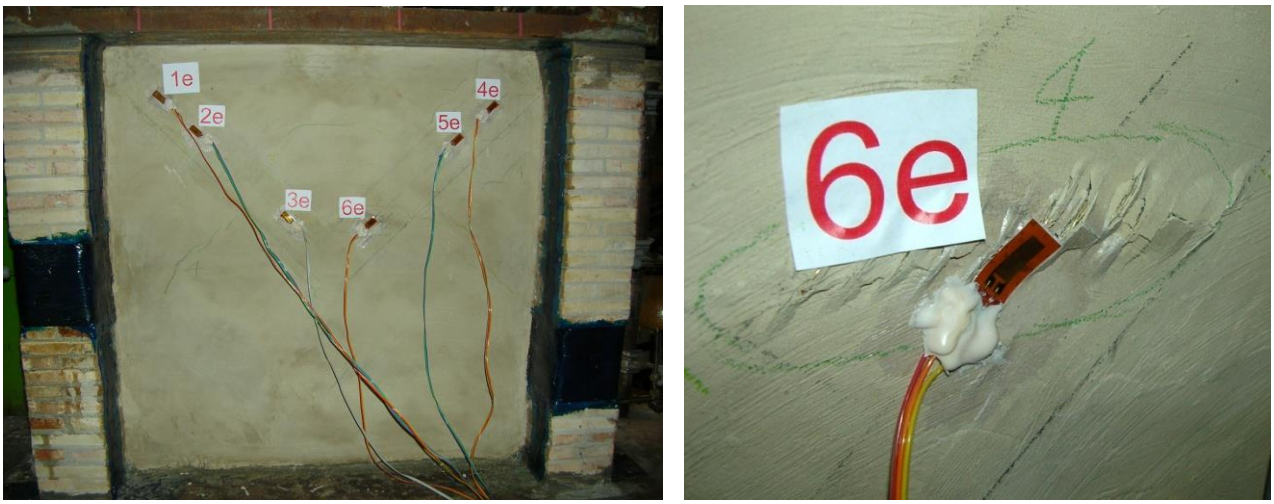

(a) (b)

Figure 29 – (a) View on reinforced side of experimental model M-LW3 with (b) local detachment view of SRG strip on point of glued strain gauge no. 6.

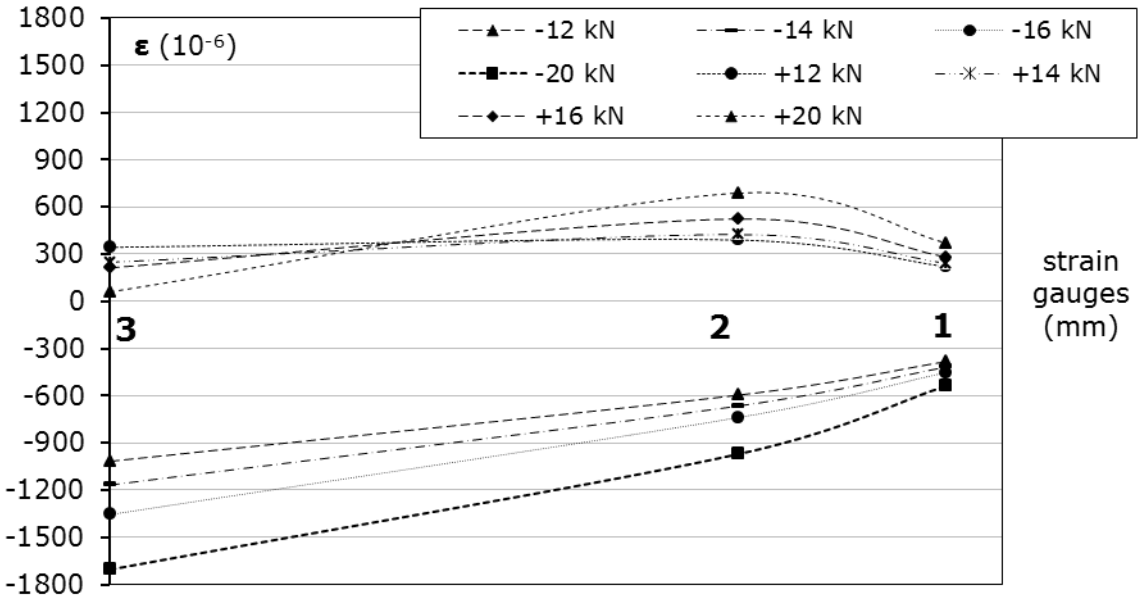

Figure 30 – Exp. values of strain at strain gauges 1,2,3 on one diagonal SRG strip in reinforced M-LW3 until cycle F=±20kN.

Under compression by alternative horizontal force, strengthening with SRG strips has shown a weak behaviour. A theoretical model which may be use to analyse the buckle response is described Below considering the SRG strip as an elastic beam embedded in an elastic medium and subjected to compressive forces, P, at the ends (Fig. 31). The strip may buckle under a system of loads due to forces P and load reactions of springs of constant k for displacement y(x). The constant has

dimension of a force on unit length and unit displacement; it depends on the width b of strips by the relation $k=k_0 \cdot b$. As known, the problem can be approached according to the energy method [30].

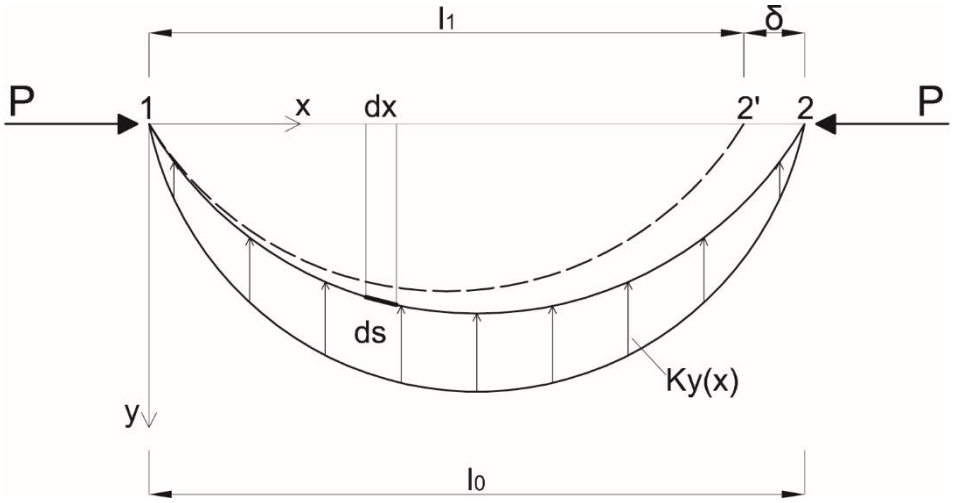

Figure 31 – Beam model for SRG strip on elastic springs under compression

Internal energy contributions due to bending of ideal beam and to response of springs for the displacement y(x) are as follows:

$$E_i = \frac{1}{2}\int_0^l EI(y'')^2 dx + \frac{1}{2}\int_0^l Ky^2 dx \tag{1}$$

The external energy contribution is due to force P multiplied by displacement δ of beam equal to the distance 2-2' (Fig. 31). It is obvious that the arches 1-2 or 1-2′ have to be the same distance 1-2, equal to l, due to small deflections y(x). The rectified length of the arc 1-2′ is the same as the straight beam 1-2; the differential length of bending beam is:

$$ds = dx\sqrt{1-y'^2} \tag{2}$$

so that the length l may be expressed as follows:

$$l = \int_0^{l-\delta} dx\sqrt{1+y'^2} = \int_0^l dx\sqrt{1+y'^2} - \int_{l-\delta}^l dx\sqrt{1+y'^2} \tag{3}$$

The Eq. (3) may be simplified as:

$$l = \int_0^l dx\sqrt{1+y'^2} - \delta \tag{4}$$

By expanding the function square root into Maclaurin series, it is derived:

$$\sqrt{1+y'^2} \cong 1+\frac{y'^2}{2} \tag{5}$$

so that the final expression for displacement is:

$$\delta = \frac{1}{2}\int_0^l (y')^2 dx \tag{6}$$

The external energy is:

$$E_e = \frac{1}{2}P\int_0^l (y')^2 dx \tag{7}$$

so that for the balance of energy from Eqs. (1) and (7) we obtain:

$$\frac{1}{2}P\int_0^l (y')^2 dx = \frac{1}{2}\int_0^l EI(y'')^2 dx + \frac{1}{2}\int_0^l Ky^2 dx \tag{8}$$

Following Rayleigh's procedure and assuming the shape of beam in equilibrium in the following way: $y(x) = y_0 sen\frac{\pi x}{l}$ the critical buckling load is:

$$P_{cr} = k\left(\frac{l}{\pi}\right)^2 + EI\left(\frac{\pi}{l}\right)^2 \tag{9}$$

The value of P_{cr} may be express as dimensionless value dividing for $\sqrt{kEI}$ and the Eq. (9) may be rewritten as:

$$\frac{P_{cr}}{\sqrt{kEI}} = t^2 + \left(\frac{1}{t}\right) \tag{10}$$

being t a new variable: $t = \frac{\sqrt{2}\beta \cdot l}{\pi}$ and β a dimension coefficient: $\beta = \sqrt[4]{\frac{k}{4EI}}$.

The function (10) has a minimum for t=1; so that the smallest load P_{cr} for any length is equal to:

$$P_{cr} = 2\sqrt{kEI} \tag{12}$$

By experimental test on M-LW3, the strain value of SRG strip on principal diagonal at the step of buckling of wires has been recorded at horizontal force equal to F=20 kN (Fig. 24) so that P_{cr} of wires of SRG strip may be estimated by:

$$P_{cr}=\varepsilon_{SRG}\cdot E_s\cdot A_{s,tot}\approx 800N \quad (13)$$

with: $\varepsilon_{SRG}\approx 1\cdot 10^{-3}$, average value on strain gauge no. 3; E_s=118GPa, Young's modulus of steel wires; $A_{s,tot}=nA_w$, total area of n=11 wires in the strip, being A_w=0.62 mm^2 area of one wire.

Comparing Eqs. (12) and (13), the constant may be evaluated equal to k≈4N/mm^2 as representative of ideal spring's modulus due to adhesion of SRG strip on masonry surface.

6. CONCLUSIONS

This paper presents an experimental investigation on four masonry models characterized by double-leaf on the web. The models were adopted to analyze the response of historical double-leaf web masonry commonly used in historical buildings. In this paper a comparison between the experimental results obtained for unreinforced and reinforced wall models having two types of composite materials - GFRP and SRG – is shown. The main results are the following:

- The walls of the unreinforced panels remain united up to failure;
- The strengthening of the GFRP equipped panels led to an increase in resistance only for one of the models investigated, M-LW4, however what is mainly observed is a strong increase in lateral deflection with increase in ductility;
- Failure of the GFRP reinforced panels occurred with cracking of the masonry and the resulting failure of the GFRP strips;
- The strengthening of the GFRP and SRG equipped panels led to an increase in deformation energy due to wider load cycles;
- The strengthening of the SRG strip equipped panel highlighted debonding mechanism resulting from local instability of the strengthening's steel wire.

The experimental results allow focusing attention on a need that the use of composite FRP materials generally does not satisfy, that is, the need to increase the resistance of the cross walls; it does however allow confiding in a major displacement capacity even if, possible, local phenomenon of instability of the same strengthening can cause brittle failure resulting from debonding mechanisms.

Acknowledgement

This research was supported by research funds provided by Polytechnic University of Marche. The authors would like to express their gratitude to the students and technicians who collaborated in the development of the experimental research.

List of symbols

A_{eq} = equivalent cross-section of FRP strip
f_{mt} = bending tensile strength of mortar
f_m = compressive strength of mortar
f_x = compressive strength of mortar parallel bed mortar joints
f_y = compressive strength of mortar normal bed mortar joints
f_b = compressive strength of brick
E_x = Young's modulus of masonry parallel bed mortar joints
E_y = Young's modulus of masonry normal bed mortar joints
F = experimental lateral load
P = compressive load
σ_{av} = average vertical stress
ε = strain
δ = lateral deflection for wall in the principal plane; displacement under compressive load.
τ_{av} = average shear stress
$_{exp}$, $_{th}$ = index for experimental value; index for theoretical value
k = modulus of springs
P_{cr} = buckling load of steel wires
E_i , E_e = internal and external energy

References

1. Codice di Pratica per gli interventi di miglioramento sismico nel restauro del patrimonio architettonico Regione Marche.(in Italian) 2007, Editors: Doglini F. and Mazzotti P.

2. Tomazevic M. Earthquake-resistant design of masonry buildings. London Imperial College Press, 1999.

3. Turnesec V., Cacovic F. Some experimental results on the strength of brick masonry walls. In: Proc. 2nd Int. Brick Masonry Conf., Stoke on Trent 1971, UK, 149-156.

4. Mann W., Muller H. Failure of shear-stressed masonry. In: Proc. of the British ceramic society. 1980. vol. 27: 223-235.

5. Magenes G, Calvi G.M. In-plane seismic response of brick masonry walls. Earthquake Eng. Struct. Dyn. 1997. **26**(11): 1091-1112.

6. Capozucca R., Sinha B.P. Strength and Behaviour of Historic Masonry under Lateral Loading. In: Proc. 13th IBMaC, Amsterdam. 2004. vol. 1: 277-284.

7. Capozucca R. Historic multiple-leaf masonry walls models under compression and cyclic shear loads. In: Proc. Int. Conf. SAHC**,** Bath, UK. 2008. vol. I: 297-302.

8. EC6. 1995. Design of Masonry Structures, Part 1-1: general rules for buildings – rules for reinforced and un-reinforced masonry ENV 1996 1-1: Bruxels: CEN.

9. Hendry A.W., Sinha B.P. Shear tests on full scale single storey brickwork structures subjected to pre-compression. Civil Engineering and Public Works Review. 1971. 1339-1334.

10. Schubert, P., Bohne. Schubfestigkeit von Mauerwerk aus Leichtbetonsteinen. das Mauerwerk Heft 3. Ernst & John 2002. 98-102.

11. Benjamin R., Williams H.A. The behaviour of one-story brick shear walls, Jour. of Struct. Division ASCE. 1958. **84**(1723): 1-30.

12. Lourenço, P. Computations of historical masonry constructions. Progress in Structural Engineering and Materials. 2002. **4**(3): 301-319.

13. Pina-Henriques, J., Lourenço, P.B., Binda, L. Anzani, A. Testing and modelling of multiple-leaf masonry walls under shear and compression. In: Proc. 4th SAHC Padua, Italy. 2004. 299-312.

14. Binda L., Pina-Henriques J., Anzani A., Fontana A., Lourenço P.B. A contribution for the understanding of load-trasfer mechanisms in multi-leaf masonry walls: testing and modelling. Eng. Strut. 2006; 28(8): 1132-48.

15. Ramalho M.A., Taliercio A., Anzani A., Binda L., Papa E. A numerical model for the description of the nonlinear behaviour of multi-leaf masonry walls. Adv. Eng. Softw. 2008. **39**(4): 249-57.

16. Triantafillou TC. Strengthening of masonry structures using epoxy-bonded FRP laminates, 1998; Jour. Composites for Construction, **2**(5): 96-104.

17. Ehsani M., Saadatmanesh H., Velazquez-Dimas J. Behavior of retrofitted URM walls under simulated earthquake loading. J. Compos. Constr. ASCE. 1999. **3**(3): 134-42.

18. Shrive NG. The use of fibre reinforced polymers to improve seismic resistance of masonry. Construction and Building Materials. 2006. **20**: 269-277.

19. Wang C., Forth J.P., Nikitas N., Sarhosis V. Retrofitting of masonry walls by using a mortar joint technique; experiments and numerical validation. Engineering Structures. 2016. **117**: 58-70.

20. Capozucca R. Experimental analysis of historic masonry walls reinforced by CFRP under in-plane cyclic loading, Composite Structures. 2011. **94**: 277-289.

21. CNR-DT 200/2004. Guide for the design and construction of externally bonded FRP systems for strengthening existing structures. 2004.

22. Foraboschi P. Strength Assessment of Masonry Arch Retrofitted using Composite Reinforcements. Masonry International. 2001. **15**(1): 17-25.

23. Borri A, Avorio A. Problemi di collegamento tra materiali FRP e strutture murarie. In: Proc. Mechanics of Mas. Struct.s Strengthened with FRP-Materials, 2000. Venezia, 179-188.

24. Aiello MA, Sciolti MS. Analysis of bond performance between FRP sheets and calcarenite stones under service and ultimate conditions. Masonry International. 2008. **21**(1): 15-28.

25. Capozucca R. Experimental FRP/SRP-historic masonry delamination. Composite Structures. 2010. **92**: 891-903.

26. Oliveira D., Basilio I., Lourenço P. Experimental bond behavior of FRP sheets glued on brick masonry. J Compos. Constr. ASCE. 2011. **15**:32-41.

27. Fedele R., Milani G. A numerical insight into the response of masonry reinforced by FRP strips. The case of perfect adhesion. Compos. Struct. 2010. **92**: 2345-57.

28. Ghiassi B., Marcari G., Oliveira D.V., Lourenço P. Numerical analysis of bond behavior between masonry bricks and composite materials. Eng. Struct. 2012. **43**: 210-20.

29. ASTM D 3039/D 3039 M - 08. Standard Test Method for Tensile Properties of Polymer Matrix Composite Materials. American Standard of Testing and Materials (2008).

30. Den Hartog J. P. Advanced Strength of Materials. Dover Publications Inc.. 1987.